J. Electrochem. Sci. Eng. **6(3)** (2016) 253-263; doi: **10.5599/jese.307**

Open Access : : ISSN 1847-9286

https://pub.iapchem.org/ojs/index.php/JESE

Original scientific paper

Preparation of NiO-graphene oxide nanosensor for adsorptive stripping voltammetric determination of dinoterbon in food samples

Kasaram Roja, Puthalapattu Reddy Prasad, Punyasamudram Sandhya*, Neelam Yugandhar Sreedhar✉

Electroanalytical Lab, Department of Chemistry, Sri Venkateswara University, Tirupati-517 502, A. P., India

**Department of Chemistry, Sri Padmavati Mahila Visvavidyalayam, Tirupati-517 502, A. P., India*

✉Corresponding Author: sreedhar_ny@rediffmail.com; Tel.: +91-877-2249666 (303)

Received: May 29, 2016; Revised: August 28, 2016; Accepted: September 9, 2016

Abstract

Graphene oxide (GO) modified NiO electrochemical nanosensor was developed for the determination of the dinoterbon in food samples using adsorptive stripping voltammetry. The modified nanosensor characterized by TEM, XRD, cyclic and adsorptive stripping voltammetry. Dinoterbon pesticide exhibited a single well-defined cathodic peak at pH 4.0 at Britton–Robinson buffer (-810.0 mV). The voltammetric characterization of the pesticide residues is evaluated and the parameter such as the effect of pH, scan rate, pulse amplitude, deposition potential and deposition time were optimized. The current–concentration plot obtained using this peak was straight-lined over the range from 0.05 to 50.00 μg mL^{-1} with limit of detection (LOD) 0.028 μg mL^{-1}. The proposed method was efficiently applied to the determination of dinoterbon in food samples. The mean recoveries of the pesticide 97.40 to 99.88 % with a relative standard deviation of 0.114 % in food samples respectively.

Keywords

Nanosensor, pesticide, voltammetry

Introduction

Wide-range usage of pesticides in agriculture, which leads to accumulation of pesticide residues in soil, water and food, has imposed a serious risk to human health and the environment worldwide [1]. Carbamates are one of the major classes of synthetic pesticides and due to their broad biological activity, these compounds are used on a large scale around the world [2]. The most commonly used

pesticide with acaricides and fungicides activity is dinoterbon (2-*tert*-butyl-4,6-dinitrophenyl ethyl carbonate), see Fig. 1. It has been used extensively by farmers on major crops and other field crops [3]. However, it is used to prevent the larvae of the pests from growing up. Dinoterbon, like all fungicide pesticides exhibits toxicity to humans, including carcinogenicity, reproductive, developmental toxicity, neurotoxicity and acute toxicity [4].

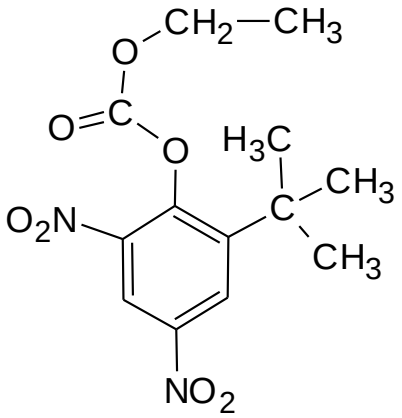

Figure 1. *Chemical structure of dinoterbon*

Graphene oxide a two-dimensional sheet of sp^2-bonded carbon atoms arranged in a honeycomb lattice, has attracted increasing attention since it was first isolated from three-dimensional graphite by mechanical exfoliation [5]. Due to its extraordinary thermal, mechanical, and electrical properties, graphene is usually considered as a competitive candidate for next generation electronic application devices such as super capacitors [6,7], batteries [8], fuel cells [9], solar cells [10], sensors [11], biosensors [12], energy storage [13] and catalysts [14]. However, many researchers have reported that the pure graphene actually exhibit unsatisfactory electrical conductivity because of the inevitable aggregation [15]. On the contrary, functionalized graphene sheets are easier to disperse in organic solvents, which can improve the dispersion and the homogeneity of the graphene with in aqueous solutions and yield novel types of electrically conductive nanocomposites [16-18]. Also, some of the useful and unique properties of graphene can only be realized after it is functionalized with organic groups such as hydroxyl, carboxyl and amino groups [19]. However, nanostructural metal oxide semiconductors possess a high surface area, nontoxicity, good biocompatibility, catalytic activity and chemical stability. Among the metal oxide semiconductors, nickel oxide (NiO), a p-type semiconductor with a wide band gap of 4.0 eV at 300 K, has been investigated for various applications such as solar cells, electrochemistry nanosensors [20,21]. Electrochemical nanosensors based voltammetric techniques have become extremely useful for the monitoring of pesticides [22,23].

In the present paper authors developed a novel NiO/GO electrochemical sensor prior to determination of dinoterbon pesticide residues at low concentration levels in food samples. The developed NiO-GO/GCE nanocomposite characterized by XRD, TEM, cyclic voltammetry and adsorptive stripping voltammetry (AdSV). Under the optimized operational conditions, the developed electrochemical nanosensor showed a specific and excellent performance with a good sensitivity, selectivity and wide dynamic range toward the quantification of dinoterbon. The results implicate the applicability of NiO/GO nanocomposite for rapid, sensitive and selective analysis of dinoterbon.

Experimental

Instrumentation and reagents

The electrochemical measurements were carried out in Autolab, three electrode systems consisting of modified glassy carbon electrode as a working electrode, Ag/AgCl (salt KCl) as a reference electrode and a platinum wire as an auxiliary electrode. Transmission electron microscopy (TEM) micrographs were performed a JEOL JEM 200CX operating at 200 kV. All reagents used were of analytical reagent grade. Ultrapure water was used throughout the experiment. The technical grade samples of dinoterbon fungicide in the form of 50 % wet-table powders were obtained from Bayer India Ltd. India.

Synthesis of nickel oxide nanocomposite

The NiO prepared from $NiNO_3 \cdot 6H_2O$ precursor by drop wise addition of 0.1 mol L^{-1}, KOH to a 0.1 M $NiNO_3 \cdot 6H_2O$ solution was kept vigorously stirred until the pH becomes 10.0. The precursor was filtered and rinsed with ultrapure water for twice and with ethanol once. Wet cake obtained was dried in oven at 100 °C overnight and was heated at 400 °C for 4 h to form black NiO nanoparticles.

Fabrication of the NiO-GO modified GCE

Before modification, the bare GCE (diameter 3 mm) was prudently polished to a mirror-like surface with 0.3, 0.05 M alumina slurries in sequence, then sonicated in ethanol and distilled water for 3 min respectively and dried with nitrogen. The 15 µL of NiO/GO suspension, prepared by simply mixing of NiO and GO suspensions with an appropriate volume ratio (v/v), was then dropped onto the clean electrode. Then the electrode was dried under room temperature, making the GO/GCE, NiO/GCE, GO and NiO-GO modified GCE.

Recommended analytical procedure for the determination of dinoterbon

An aliquot of working standard solution containing 5.0 µg mL^{-1} of dinoterbon pesticide is taken into 25 mL volumetric flask. To this 5 mL of Britton-Robinson buffer of (pH 4.0) added and transferred into electrolytic cell and diluted with 9.0 mL of supporting electrolyte and then deoxygenated with nitrogen gas for 5 min. The pesticide residue was treated with electrochemical NiO-GO nanocomposite on the surface of glassy carbon electrode. The dinoterbon pesticides were determined by cyclic and AdSV mode. Electrolysis was done at +0.8 to -1.20 V *vs.* SCE, accumulation time 80 s, pulse amplitude of 25 mV, scan rate 20 mV s^{-1} and pH 4.0. The maximum voltammetric peaks appearing for sample is at -0.810 V for dinoterbon.

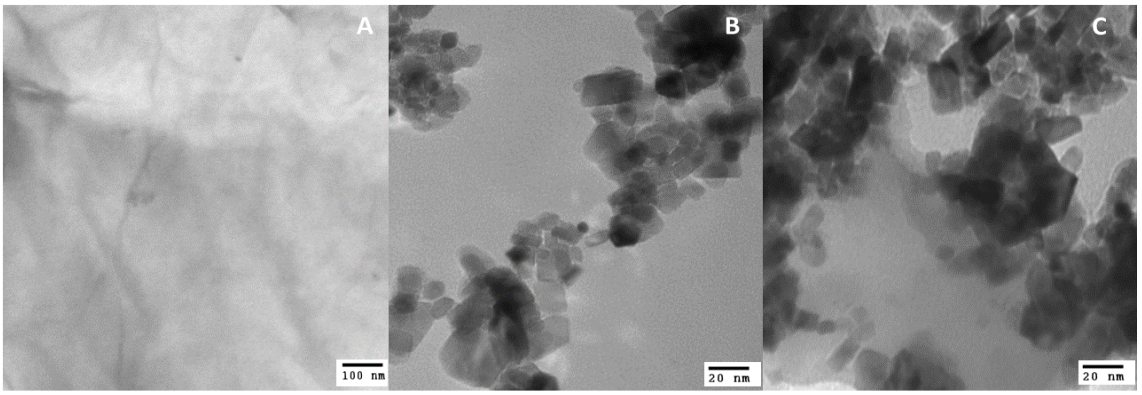

Figure 2. *TEM images of GO (A), NiO (B) and NiO/GO (C) modified glassy carbon electrode.*

Results and discussion

The structure of the GO fabricated NiO nanocomposite was examined by TEM and XRD. The morphological structure of the resulting NiO/GO was investigated by TEM (Fig. 2). The TEM image of single layer graphene oxide as shown in Fig. 2A. Fig. 2B, shows the TEM image of many NiO nanoparticles with sphere-like morphology are homogeneously dispersed. The many NiO nanoparticles with sphere-like morphology are homogeneously anchored on the surface of the GO sheets as shown in Fig 2C. The revealing sphere-like NiO nanoparticles with an average size of 28.6 nm. The XRD was used to investigate the phase structure of the resulting hybrids (Fig. 3). Fig. 3a shows the X-ray diffraction spectrum of NiO samples. The XRD patterns exhibit five prominent peaks at 2θ = 37.4°, 43.3°, 63.5°, 75.4° and 79.6° can be readily indexed as (111), (200), (220), (311) and (222) crystal planes of the bulk NiO, respectively. Fig. 3b shows the X-ray diffraction spectrum of GO fabricated NiO nanocomposite. The XRD pattern of the NiO/GO hybrid exhibits crystalline NiO diffraction peaks, which are in good agreement with the standard NiO (JCPDS No. 04-0835). The as-prepared GO displays a characteristic (002) peak at 25.4 which is in good agreement with previous reports [24]. By applying the Scherer formula to the XRD peaks, the average crystal size was calculated to be 22.4 nm for the nickel crystalline particles. This result indicates that the intermediate products was completely converted to NiO, which can be indexed as disordered stacked graphitic sheets. This finding indicates that GO is similar to previous reports [25].

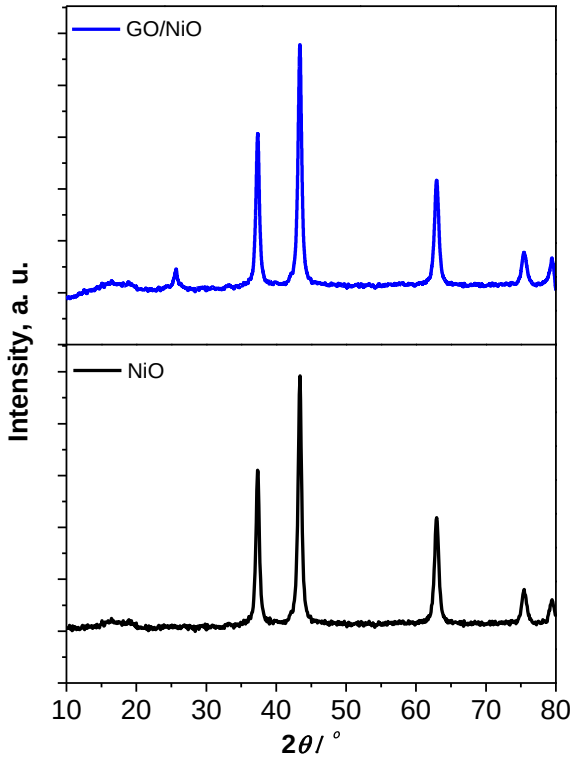

Figure 3. *XRD patterns of NiO and GO-NiO nanocomposite*

Voltammetric response of dinoterbon at various electrodes

The electrochemical performance of various electrodes was first investigated by cyclic voltammetry. Fig. 4, showed the cyclic voltammetry of the bare GCE, GO/GCE, NiO/GCE and NiO-GO/GCE in 0.1 M pH 4.0 BR buffer solution in the presence of 5.0 μg mL^{-1} dinoterbon. There was no obvious peak observed at bare GCE. However, a cathodic peak response at −0.810 V was observed at the NiO/GCE and GO/GCE, respectively. According to the currently accepted mechanism [24,25], the

reduction peak should be attributed to a four-electron transfer reduction of the each nitro group (-NO_2) to give the hydroxylamine derivative. It can be reoxidized to the nitroso compound at a more positive potential. Under subsequent cycling, the nitroso group was reversibly reduced to respective hydroxylamine. Consequently, the redox behaviors of dinoterbon at the NiO-GO electrode is shown in scheme. 1.

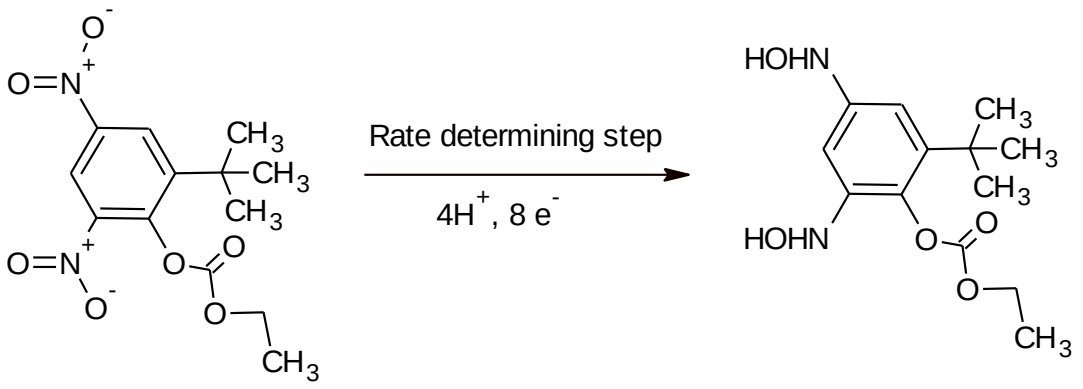

Scheme 1. *Reduction mechanism of dinoterbon*

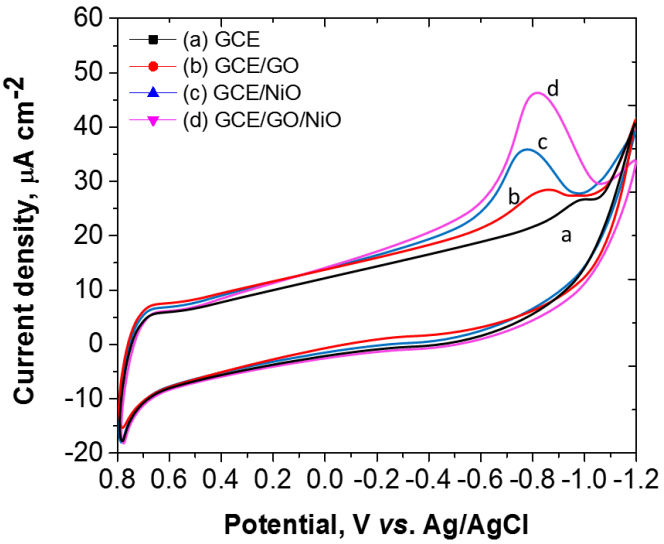

Figure 4. *Typical cyclic voltammogram of dinoterbon for an accumulation time of 80 sec at GCE (a); GO/GCE (b); NiO/GCE (c); NiO-GO/GCE(d); rest time: 10 s; scan rate: 20 mVs^{-1}; concentration: 5.0 µg mL^{-1}; pH: 4.0 (BR buffer); pulse amplitude: 25 mV.*

The NiO-GO/GCE strong cathodic peak current response at -0.810 V, which was more prominent than those obtained at the bare GCE, NiO/GCE and GO/GCE. Furthermore, one can see that the incorporation of NiO into GO nanocomposite possesses more prominent peaks, indicating that the use of GO can significantly enhance the electron transfer between NiO-GO and the GC electrode. The normalized signal response of the different electrodes to 5.0 µg mL^{-1} dinoterbon were calculated. The dinoterbon response at the NiO-GO/GCE is more than the normalized response at the NiO/GCE and GO/GCE. These showed the NiO/GO/GCE gave the highest normalized signal response. The enhanced performance of the NiO-GO/GCE nanocomposite can be attributed to the excellent affinity of dinoterbon with NiO and the enhanced electron transfer, which could amplify the interaction between dinoterbon and NiO due to the formation of entangled NiO-GO structure.

The difference in the electrochemical behaviour of dinoterbon at bare GCE, GO/GCE and NiOGO/GCE were also evaluated by AdSV in 0.1 mol L-1 BR buffer pH 4.0, containing 20 µg mL-1 dinoterbon, at scan rate of 20 mV s–1 (Fig. 5).

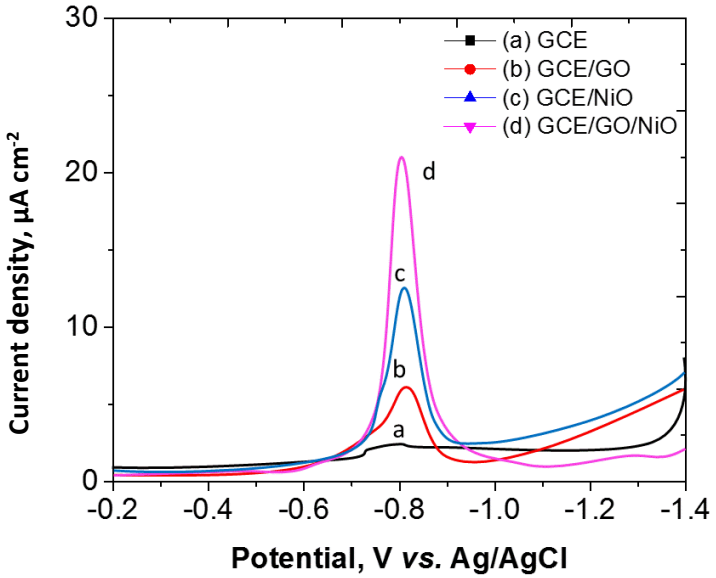

Figure 5. *Adsorptive stripping voltammogram of dinoterbon at bare GCE (a), GCE/GO (b), GCE/NiO (c), NiO-GO/GC electrode(d); pH 4.0 (BR buffer) accumulation time: 80 s.; stirring rate: 1500 rpm; scan rate:20 mVs^{-1}; pulse amplitude: 25 mV.*

No characteristic peak related to the dinoterbon reduction was observed for the bare glassy carbon electrode which indicates GCE does not exhibit electrocatalytic activity for dinoterbon. However, when the determination was performed at the GO/GCE, NiO/GCE and NiO-GO/GCE electrodes, there was a peak for dinoterbon at -0.713 and -0.688 V, respectively. These peaks indicate that both GO/GCE and NiO-GO/GCE electrodes exhibit electrocatalytic activity and can identify the fungicide dinoterbon. However, the electrode modified with the hybrid material, NiO-GO/GCE, showed a well electrocatalytic response with higher catalytic current and the potential was less positive compared to the other modified electrodes. It can be explained due to the GO physically incorporated into the NiO nanocomposite were oriented in such a way that their extremities were more susceptible to reacting with the fungicide dinoterbon.

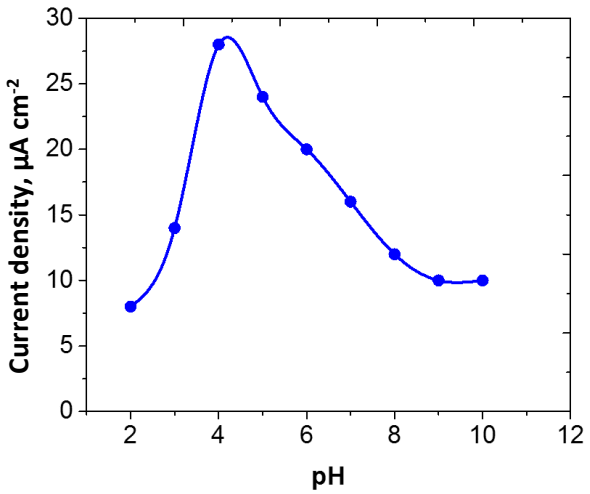

Figure 6. *Effect of pH on dinoterbon at NiO-GCE/GCE; accumulation time: 80 s.; rest time: 10 s., stirring rate: 1500 rpm; scan rate: 20 mVs^{-1}; concentration: 5.0 µg mL^{-1}; pulse amplitude: 25 mV.*

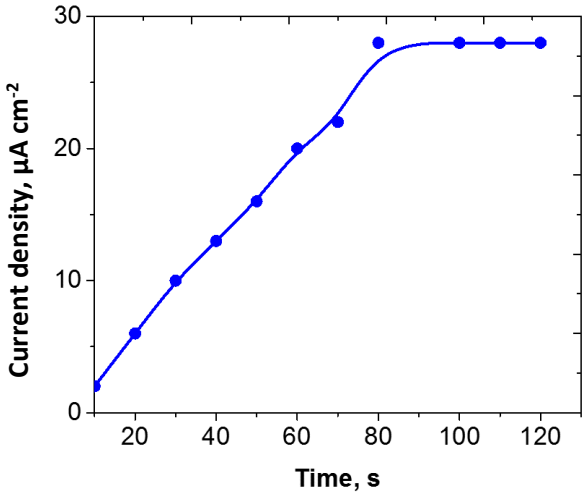

Figure 7*. Effect of accumulation time on the AdSV response of dinoterbon at NiO-GO/GCE; rest time:10 s; stirring rate: 1500 rpm; scan rate: 20 mVs^{-1}; concentration: 5.0 µg mL^{-1}; pH: 4.0 (BR buffer); pulse amplitude: 25mV.*

Optimization parameters for dinoterbon detection at NiO-GO/GCE

The peaks of AdSV for dinoterbon (20 μg mL^{-1}) with NiO-GO/GCE were compared in different supporting electrolytes, namely, 0.1 mol L^{-1} Britton–Robinson buffer, 0.2 mol L^{-1} sodium acetate–acetic acid buffer, 0.1 mol L^{-1} phosphate buffer, carbonate buffer, and borate buffer solution. The highest peak current was obtained with 0.1 mol L^{-1} Britton–Robinson buffer as the electrolyte. Thus, 0.1 mol L-1 Britton–Robinson buffer was chosen as the analytical medium, in which the peak shape was well defined. As shown in Fig. 6, the effects of pH on the AdSV peak current of dinoterbon (20 μg mL^{-1}) with NiO-GO/GCE was also studied in 0.1 M Britton–Robinson buffer (pH 2.0–10.0). The maximum current appeared at pH 4.0 for the determination of dinoterbon. In the following experiment, pH 4.0 was selected.

Further investigation of electroactivities using the various ratios of NiO to GO was preliminarily studied to optimise the catalytic performance of NiO-GO/GCE toward dinoterbon. The mass ratio of NiO:GO was varied from 1:0.25 to 1:0.5, 1:1, 1:2, and 1:4; the highest peak current was obtained at a mass ratio of 1:2. The catalytic activity of the as-prepared NiO-GO hybrid for dinoterbon reduction was under the synergistic effect of the primary component (NiO) and the support component (GO). The combination of GO with NiO is an ideal strategy of improving the catalytic performance of NiO by enhancing its charge transfer efficiency. However, excessive GO in the composite can also decrease the loading level of NiO. Thus, the mass ratio of NiO-GO has an important influence on the catalytic oxidation reactions of dinoterbon. The optimum catalytic performance was achieved from NiO-GO with a mass ratio of 1:2. The excellent adsorption capacity of GO, (2) the larger effective surface area of NiO-GO/GCE, and (3) the synergistic catalytic effect of GO, and NiO toward dinoterbon, as detailed above.

The AdSV peak current of dinoterbon increases with accumulation time increasing from 0 to 80 s, as shown in Fig. 7. But when it exceeds 80 s the peak current remains almost constant for a 5.0 μg mL^{-1} dinoterbon solution, meaning that an accumulation/or extraction equilibrium is achieved at the electrode/solution interface. The influence of accumulation potential is examined from +0.3 to −0.5 V. The results showed that the peak current of dinoterbon is almost independent of accumulation potential. This is due to the neutral nature of dinoterbon under this condition. Thus, an accumulation is performed under open-circuit.

The effect of pulse height variation on the peak current of dinoterbon voltammograms was studied in the range of 15–100 mV. The obtained results showed that increasing the pulse heights up to 25 mV will cause an increase in peak current. Pulse heights more than 25 mV cause broadening of the dinoterbon voltammogram and so decreasing the peak current intensity of the analyte. So the optimum pulse height value was selected to be 25 mV.

Table 1. *Tolerance limits of matrix substances for determination of dinoterbon by the AdSV method*

substances	Tolerance limit, μg mL^{-1}	substances	Tolerance limit, μg mL^{-1}
Na^+, K^+, NH_4^+	1200	Cu^{2+}, Cr^{6+}	60
Ca^{2+}, Mg^{2+}	1000	Phenols and nitrophenols	50
Cl^-, NO_3^-, HCO_3^-	800		
PO_4^-, SO_4^{2-}	750		
Al^{3+}, Zn^{2+}, Fe(II)	400		

Interference study

Prior to the application of the developed method on food samples it was vital to investigate the effect of some of the interfering ions on the recovery percentage of dinoterbon. The AdSV

determination of dinoterbon was tested in the presence of spiked known amounts of interfering ions and molecules. The tolerance limit was defined as the amount of the foreign substance causing a change of ±5 % in the peak current intensity reading. The tolerable limits of interfering substance are given in Table 1. The results showed that most of the investigated substances do not interfere in the AdSV determination of dinoterbon in food samples

Determination of dinoterbon pesticide in food samples

The food samples namely, Onion (*Alium sepa*), Cauliflower (*Brassica olera. var. Botrytis*), Lady's Finger *(Abelmoschus esculentus)*, Cucumber (*Cucumis sativus*), Sweet Potato (*Ipomoea*) and Tomato (*Lycopersicum esculentum*) were collected from the Tirupati local market, A.P, India. Afterwards, they were taken in small mesh and dried in an oven at 90 °C to constant weight. In order to digest the samples, 1.0 g of food sample was digested with 10 mL concentrated HNO_3 (65 %) and 3.0 mL H_2O_2 (30 %) in microwave system, then again evaporated to near dryness. After evaporation, 10 mL of deionized water was added and the sample was mixed. The resulting mixture was filtered through filter paper. The filtrate was diluted to 25 mL with deionized water. All the samples were stored in polyethylene bottles. For sample analysis spiked with dinoterbon standards at 10.0, 50.0, 100 µg mL^{-1}. Then 10 µg mL^{-1} of the digested sample solution was dissolved in 25 µL BR buffer solution at pH 4.0 for determination. Samples were also analyzed by GC methods. The recovery rates in food samples exhibited a range of 97.40 to 99.88 % (average of five determinations) with less than 1.72 % of RSD and precision data are reported in Table 2.

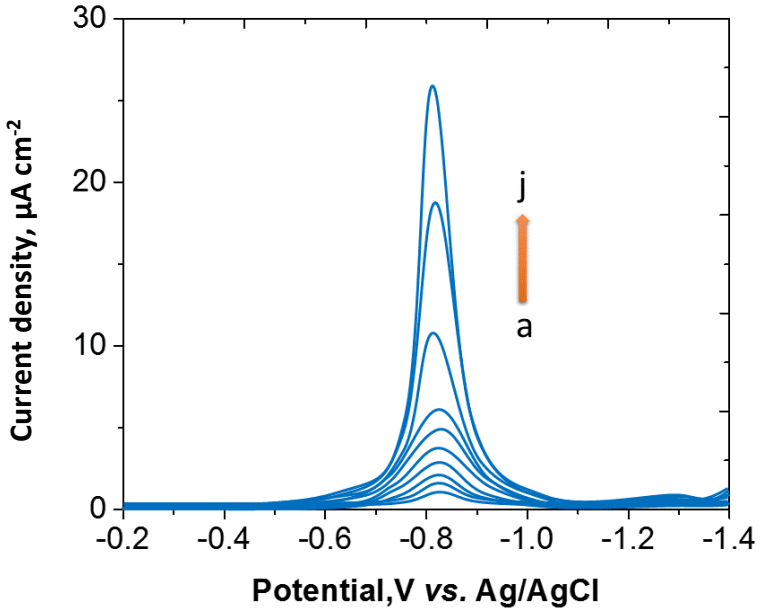

Figure 8. *AdSV of the NiO-GO/GCE by (a) 0.2, (b) 0.4, (c) 0.8, (d) 1.0 (e) 2.0 (f) 4.0, (g) 8.0, (h) 16, (i) 32 (j) 50 µg mL^{-1} dinoterbon; accumulation time of 80 s, stirring rate:1500 rpm; scan rate: 20 mVs^{-1}; pH: 4.0 (BR buffer); pulse amplitude:25 mV.*

Adsorptive stripping voltammetric quantification of dinoterbon

Due to the good sensitivity of adsorptive stripping voltammetry was applied for further electrochemical detection of dinoterbon under the optimized operating conditions. Fig. 8, displayed the AdSV of the NiO-GO/GCE in 0.1 mol L^{-1} pH 4.0 BR buffer solution at a potential range from −0.4 V to 0.2 V in the presence of various dinoterbon concentrations. Well-defined peaks, proportional to the concentration of the corresponding dinoterbon, were observed in plots. The corresponding calibration plot was presented in Fig. 9, indicating that the response was gradually saturated at a

higher dinoterbon concentration. Under the optimal experimental conditions, NiO–GO/GCE was used to detect dinoterbon by AdSV. It can be seen from the figure that well-defined AdSV responses from adsorbed dinoterbon were observed and increased gradually with the increase of the dinoterbon concentration. The good linear relationship between oxidation current and log *C* dinoterbon was obtained from 0.05 µg mL^{-1} to 50.0 µg mL^{-1} with the regression equation of *i* / µA = 0.4742x+0.1283 (R = 0.9992). A LOD of 0.0283 µg mL^{-1} was calculated according to the formula LOD = 3 σ/S, where σ is the mean of standard deviation of five measurements taken from the signal obtained from the blank, S is the slope of the calibration curve, and the number 3 comes from the required ~98 % level of confidence in the difference between the observed signal and the blank response.

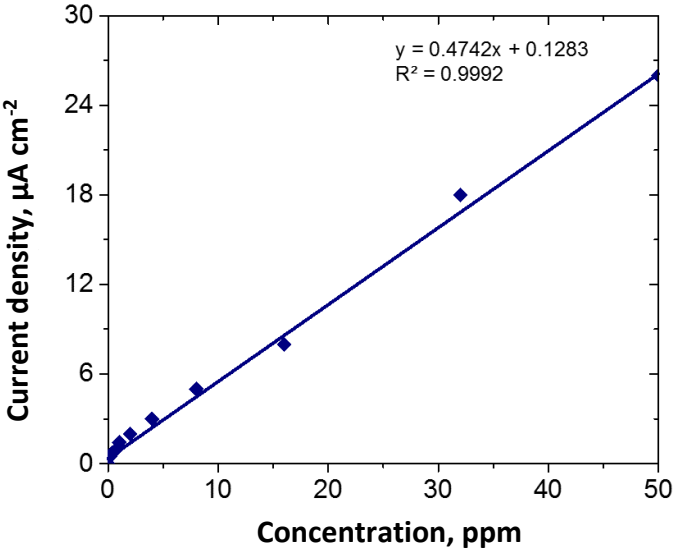

Figure 9. *Calibration curve on the AdSV response of dinoterbon at NiO-GO/GCE; 5.0 µg mL^{-1}; accumulation time of 80 s, stirring rate: 1500 rpm; scan rate: 20 mV s^{-1}; pH: 4.0 (BR buffer); pulse amplitude: 25 mV.*

Table 2. *AdSV determination of pesticide in food samples (no. of determinations =5)*

Name of the food samples	Amount added, µg mL^{-1}	Amount found, µg mL^{-1}	Recovery, %	R.S.D*
Onion	5.0	4.98	99.60	0.11
	10.0	9.92	99.20	0.08
	25.0	24.96	99.84	0.16
Cauliflower	5.0	4.87	97.40	0.02
	10.0	9.94	99.40	0.12
	25.0	24.82	99.28	0.14
Cucumber	5.0	4.88	97.60	0.22
	10.0	9.94	99.40	0.04
	25.0	24.96	99.84	0.16
Sweet Potato	5.0	4.91	98.20	0.12
	10.0	9.89	98.90	0.05
	25.0	24.97	99.88	0.20
Tomato	5.0	4.99	99.80	0.16
	10.0	9.93	99.30	0.08
	25.0	24.89	99.56	0.06

*R.S.D: Relative standard deviation

The inter-assay precision was estimated at six different NiO-GO a nanocomposite modified electrodes for the determinations in 0.1 mol L^{-1} BR buffer (pH = 4.0) containing 5.0 µg L^{-1} dinoterbon.

Similarly, the intra-assay precision was evaluated by assaying one working electrode for five replicate determinations under unvarying conditions. The relative standard deviation values of inter-assay and intra-assay were found to be 6.8% and 4.6%, respectively, indicating acceptable precision and reproducibility. In addition, the developed electrochemical metal oxide nanosensor (NiO-GO) was very stable at room temperature. No obvious decrease in the electrochemical response was observed in the 5 days and over ~90% of the initial response remained after four weeks, indicating that is acceptable stability.

Conclusions

In this paper, combining the advantageous characteristics of dinoterbon at NiO/GCE, GO/GCE and the NiO-GO/GCE nanocomposite have been prepared. The NiO-GO/GCE nanocomposite with excellent electrocatlytic and between NiO and GO modified electrode. It's improved the absorptivity and charge transfer properties on the surface of nanocomposite and improve the stability. The constructed NiO-GO/GCE sensor exhibited many advantages such as low applied potential, good fabrication reproducibility, acceptable stability, fast response and low detection limit. The NiO-GO/GCE sensor has potential application in monitoring of dinoterbon in food samples.

References

[1] R. C. Gupta, *Toxicol. Mechan. Methods*, **14** (2004) 103-143
[2] W. T. Song, Y. Q. Zhang, G. J. Li, H. Y. Chen, H. Wang, Q. Zhao, D. He, C. Zhao, L. Ding, *Food Chem*. **143** (2014) 192-198
[3] P. Lautala, M. Kivimaa, H. Salomies, E. Elovaara, J. Taskinen, *Eur. J. Pharm. Sci.* **4** (1996) S167-168
[4] X. Guo, Z. Wang, S. Zhou, *Talanta* **6** (2004) 135-139
[5] K. S. Novoselov, A. K. Geim, S. V. Morozov, D. Jiang, Y. Zhang, S. V. Dubonos, I. V. Grigorieva, A. A. Firsov, *Science* **306** (2004) 666-669
[6] M. D. Stoller, S. J. Park, Y. W. Zhu, J. H. An, R. S. Ruoff, *Nano Letters* **8** (2008) 3498-3502
[7] A. K. Mishra, S. Ramaprabhu, *Journal of Physical Chemistry C*, **115** (2011) 14006-14013
[8] E. Yoo, J. Kim, E. Hosono, H. S. Zhou, T. Kudo, I. Honma, *Nano Letters* **8** (2008) 2277-2282
[9] J. Xiao, D. Mei, X. Li, W. Xu, D. Wang, G. L. Graff, W. D. Bennett, Z. Nie, *Nano Letters* **11** (2011) 5071-5078
[10] X. Wang, L.J. Zhi, N. Tsao, Z. Tomovic, J.L. Li, K. Mullen, *Angew and te Chemie International Edition* **47** (2008) 2990-2992
[11] S. J. Guo, S. J. Dong, *Journal of Materials Chemistry* **21** (2011) 18503-18516
[12] J. D. Qiu, J. Huang, R. P. Liang, *Sensors and Actuators B* **160** (2011) 287-294
[13] D. Chen, L. H. Tang, J. H. Li, *Chemical Society Reviews* **39** (2010) 3157-3180
[14] S. S. Han, H. Kim, N. Park, *Journal of Physical Chemistry* **C115** (2011) 24696-24701.
[15] D. Li, R. B. Kaner, *Science* **320** (2008) 1170-1171
[16] S. Stankovich, D. A. Dikin, G. H. B. Dommett, K.M. Kohlhaas, E.J. Zimney, E.A. Stach, R.D. Piner, S.T. Nguyen, R.S. Ruoff, *Nature* **442** (2006) 282-286
[17] D. Li, R. B. Kaner, *Science* **320** (2008) 1170-1171.
[18] K. Wang, Q. Liu, L.N. Dai, J.J. Yan, C. Ju, B.J. Qiu, X.Y. Wu, *Analytica Chimica Acta,* **695** (2011) 81-84
[19] D. Zheng, S. K. Vashist, K. Al-Rubeaan, J.H.T. Luong, F.S. Sheu, *Talanta,* **99** (2012) 22-28
[20] T. Seto, H. Akinaga, F. Talano, K. Koga, T. Orii, M. Hirasawa, *J.Phys. Chem.B* **109** (2005)13403-13405
[21] P. Lunkenheimer, A. Loidl, C. Ottermann, H. Bange, *Phys.Rev.B:Condens. Matter* **44** (1991) 5927-5930

[22] C. N. Reddy, P. R. Prasad, and N.Y. Sreedhar, *Journal of Analytical Methods in Chemistry* **2013** (2013) 1-7
[23] D. Rekha, N. Y. Sreedhar, P.R. Prasad, *Global journal of frontier Science research*, **10** (2010) 21-29
[24] Y. Li, B. Zhang, J.X. Zhao, Z. Ge, X. Zhao, L. Zou, *Applied Surface Science* **279** (2013) 367-373
[25] H. Zhang, H. Huang, H. Ming, H. Li, L. Zhang, Y. Liu and Z. Kang, *J. Mater. Chem.*, **22** (2012) 10501-10506